Supplemental Material

Table S1. Materials properties used in 2-D numerical experiments.

Figure S1. Numerical modelling results of temperature by I2VIS for Jiaodong of E China at c. 120 Ma (a), SE coast of China at c. 105 Ma (b), N America at c. 120 Ma (c), S Peru (d) and N Chile at 110 Ma (e).

Figure S2. Numerical modelling results of bulk strain by I2VIS for Jiaodong of E China at c. 120 Ma (a), SE coast of China at c. 105 Ma (b), N America at c. 120 Ma (c), S Peru (d) and N Chile at 110 Ma (e).

Figure S3. Numerical modelling results by I2VIS for present (0 Ma) S America (a) and Solomon Islands (b).

Supplemental Text. Reconstructing plate kinetics using GPlates and Rheological model.

Table S1. Materials properties used in 2-D numerical experiments

Material	ρ_0 (kg/m^3)	k W/(m K)	H_r $(\mu W/m^3$ $\mu W/m^3)$	Flow law	E (kJ/mol)	n	A_D $(MPa^{-n}s^{-1})$	V $(J/(MPa\cdot mol))$	$\sin(\phi)$	μ (GPa)
Sediments	2700	$0.64 + \dfrac{807}{T+77}$	2.0	Wet quartzite	154	2.3	3.2×10^{-4}	0	0.03	10
Upper continental crust	2700	$0.64 + \dfrac{807}{T+77}$	1.0	Wet quartzite	154	2.3	3.2×10^{-4}	8	0.15	10
Lower continental crust	2900	$1.18 + \dfrac{474}{T+77}$	0.25	Plagioclase	238	3.2	3.3×10^{-4}	12	0.15	25
Oceanic crust	3100	$0.64 + \dfrac{807}{T+77}$	0.25	Wet quartzite	154	2.3	3.2×10^{-4}	8	0.3	25
Continental lithospheric mantle	3350	$0.73 + \dfrac{1293}{T+77}$	0.022	Dry olivine	532	3.5	2.5×10^{4}	10	0.6	67
Oceanic lithospheric mantle	3370	$0.73 + \dfrac{1293}{T+77}$	0.022	Dry olivine	532	3.5	2.5×10^{4}	12	0.6	67
Asthenosphere	3350	$0.73 + \dfrac{1293}{T+77}$	0.022	Dry olivine	532	3.5	2.5×10^{4}	10	0.6	67
Weak zone	3200	$0.73 + \dfrac{1293}{T+77}$	0.022	Wet olivine	137	1.9	2.0×10^{-4}	0	0.03	67
Reference[a]	1	2	3	4	4	4	4	4	4	3

[a] 1=(Bittner and Schmeling, 1995); 2=(Clauser and Huenges, 1995); 3=(Turcotte and Schubert, 2002); 4=(Ranalli, 1995)

Fig. S1 Numerical modelling results of temperature by I2VIS for Jiaodong of E China at c. 120 Ma (a), SE coast of China at c. 105 Ma (b), N America at c. 120 Ma (c), S Peru (d) and N Chile at 110 Ma (e).
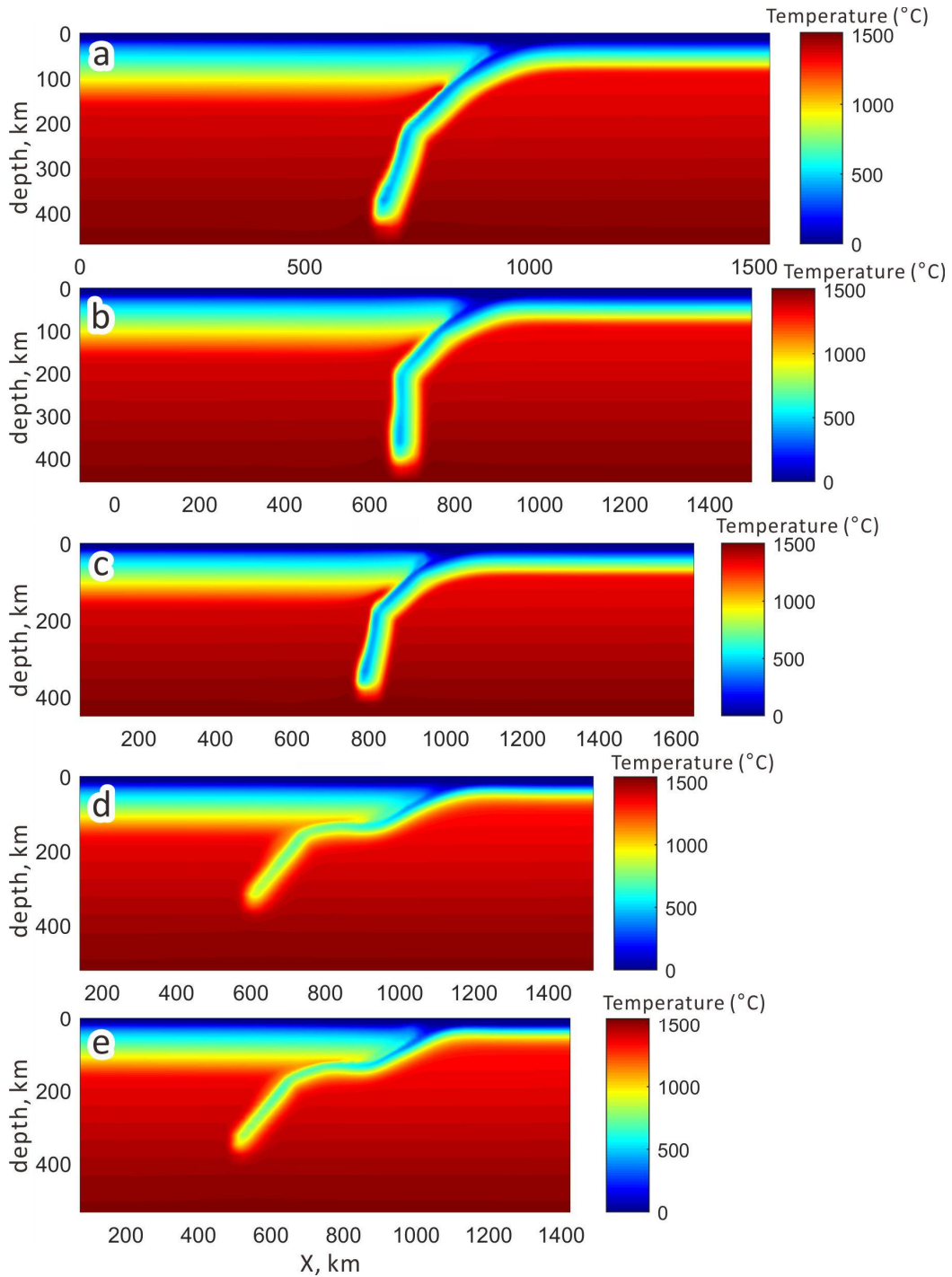
Fig. S2 Numerical modelling results of bulk strain by I2VIS for Jiaodong of E China at c. 120 Ma (a), SE coast of China at c. 105 Ma (b), N America at c. 120 Ma (c), S Peru (d) and N Chile at 110 Ma (e).
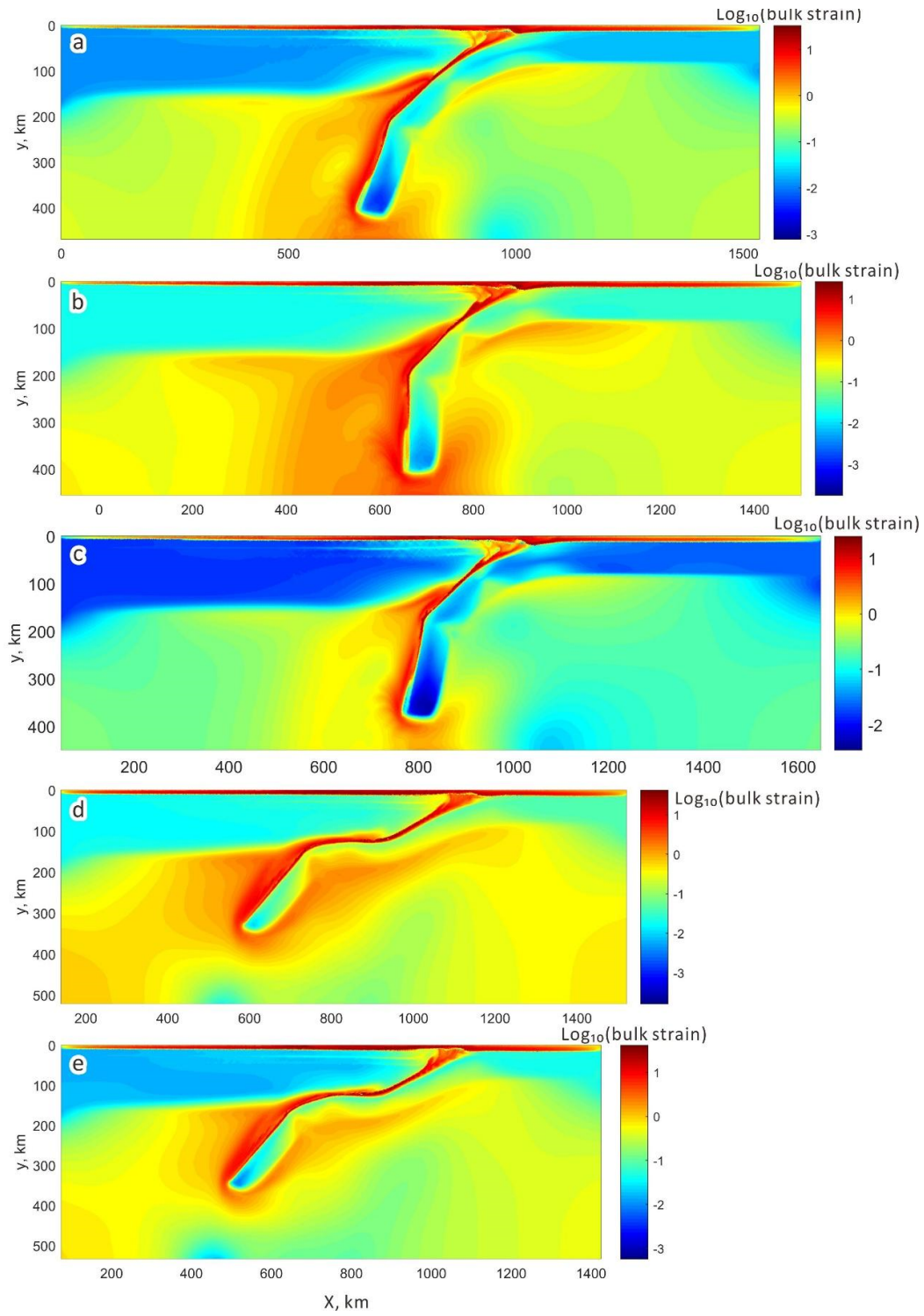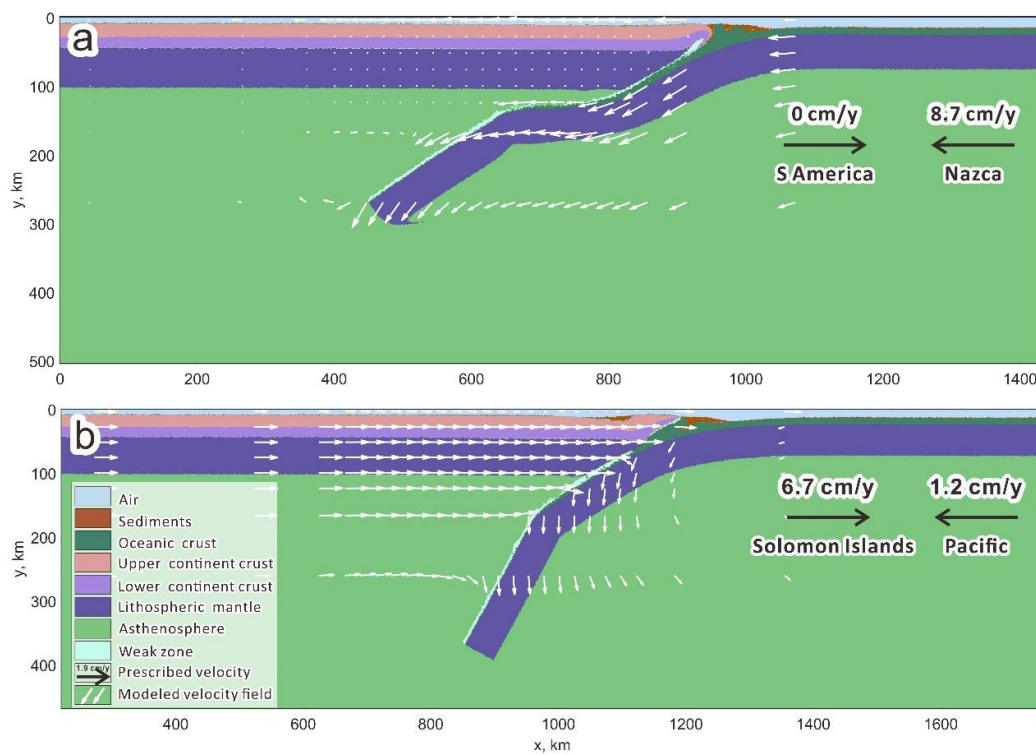
Fig. S3 Numerical modelling results by I2VIS for present (0 Ma) S America (a) and Solomon Islands (b). The prescribed velocities of oceanic slab and continent (black arrows) are calculated as the normal components of velocity vector by GPlates. Also shown are the velocity fields (white arrows). The initial modeling has a weak hydrated slab interface with an initial angle of 30°. The average ages of oceanic lithosphere are c. 20 Ma for S America and 100 Ma for the Solomon Islands arc based on the reconstructions by GPlates. The average ages of the continental lithosphere are prescribed to be 1000 Ma for S America and Solomon Islands to satisfy the high plate strength facilitating the asymmetric plate movement (Gerya et al., 2008). Note that the modelling reproduced the modern flat subduction in South America, and the intermediate-dip subduction in the Solomon Islands, consistent with present-day slab dips in South America (c. 15°) and Solomon Islands (c. 33°) determined by Slab2 (Hayes et al., 2018), providing a first-order support to the simulations of our study.

SUPPLEMENTAL TEXT

Reconstructing plate kinetics using GPlates

The GPlates virtual globe software is an open-source, cross-platform plate tectonic geographic information system (GIS), which enables end-users to explore topological plate models representing the mosaic of evolving plate boundary networks through time (Müller et al., 2018; Seton et al., 2012). GPlates stores the geometry of features (e.g., points, polylines, and polygons) in their present-day coordinates, and reconstructs them backward in time based on rotation models. The plate identification numbers (Plate ID) are assigned to features to allow the retrieval of parameter of rotation stored in a rotation file (Müller et al., 2016). The motion of all plates is tied to Africa numerically using a finite Euler rotation via plate motion chains, because of the minimal motion of Africa since Pangea (Matthews et al.,

2016). Then, the motion of Africa is linked to the base of the mantle via a true polar wander-corrected absolute reference frame model (Matthews et al., 2016). However, Pacific and associated plates, such as the Farallon, Izanagi, Phoenix, lack a shared seafloor spreading center with West Antarctica, thus the Pacific hotspot reference frame is adopted for the Pacific plate assuming that the Pacific reference frame is fixed relative to other hotspots (Seton et al., 2012).

A global set of seafloor spreading isochrones and age-grids are integrated in GPlates, based on magnetic anomaly identifications, spreading ridge locations and boundary locations defining the transition from continental to oceanic crust (Müller et al., 2008; Seton et al., 2012). The continuously closing plate (CCP) methodology is built in the GPlates to ensure that each polygon keeps topologically closed with evolving time (Gurnis et al., 2012). By means of CCP method, the plate polygons are constructed using present day plate boundaries, geological evidence for locations of arcs, sutures and major faults through time along with plate motion vectors based on our kinematic model (Bird, 2003; Seton et al., 2012). Note that the present-day continents (white polygons) in deep-time plate reconstructions are outlined by present coastlines for easy understanding, although paleo-shorelines are an additional geometric feature that can better represent the paleogeographic reconstruction (Zahirovic et al., 2016). The Kinematics Tool in GPlates provides an interactive way of visualizing latitude, longitude, and the relative or absolute plate motion velocity history of any point of interest.

Modeling slab subduction using I2VIS

I2VIS is a finite-difference numerical code with marker-in-cell technique (Gerya and Yuen, 2003, 2007), which solves the thermal and chemical buoyant forces based on momentum, continuity and heat conservation equations for a 2D creeping flow (Huangfu et al., 2018; Huangfu et al., 2016a; Li et al., 2011).

Governing equations

2D stokes equations:

$$\frac{\partial \sigma'_{xx}}{\partial x} + \frac{\partial \sigma'_{xz}}{\partial z} = \frac{\partial P}{\partial x}$$

$$\frac{\partial \sigma'_{zx}}{\partial x} + \frac{\partial \sigma'_{zz}}{\partial z} = \frac{\partial P}{\partial z} - g\rho(C, M, P, T)$$

where *x* and *z* are horizontal and vertical coordinates, respectively, g is gravitational acceleration, σ'_{ij} are components of deviatoric stress tensor, and the density ρ depends on composition (*C*), melt fraction (*M*), temperature (*T*), and pressure (*P*).

Incompressible continuity equation:

$$\frac{\partial v_x}{\partial x} + \frac{\partial v_z}{\partial z} = 0$$

where v_x and v_z are horizontal and vertical velocity components, respectively.

Heat conservation equations:

$$\rho C_P \left(\frac{DT}{Dt}\right) = -\frac{\partial q_x}{\partial x} - \frac{\partial q_z}{\partial z} + H_r + H_a + H_s$$

$$q_x = -k(T,P,c)\frac{\partial T}{\partial x} \qquad q_z = -k(T,P,c)\frac{\partial T}{\partial z}$$

$$H_a = T\alpha\frac{dP}{dt} \quad H_s = \sigma'_{xx}\dot{\varepsilon}_{xx} + \sigma'_{zz}\dot{\varepsilon}_{zz} + 2\sigma'_{xz}\dot{\varepsilon}_{xz}$$

where C_P is the effective isobaric heat capacity, i.e., incorporating latent heat, DT/Dt is the substantive time derivative of temperature, q_x and q_z are heat flux components, H_r, H_a, and H_s denote radioactive heat production, the energetic effect of isothermal compression/decompression (i.e., adiabatic heating/cooling), and shear heating, respectively, $k(T, P, c)$ is the thermal conductivity as a function of temperature, pressure, and composition (Hofmeister, 1999), α is thermal expansion coefficient, and $\dot{\varepsilon}_{ij}$ is the strain rate tensor.

Rheological model:

Rheological model

The relationship between the deviatoric stress (σ'_{ij}) and the strain rate ($\dot{\varepsilon}_{xx}\dot{\varepsilon}_{xx}$) tensors are described by realistic visco-plastic constitutive laws. In case of incompressible viscous deformation, the viscous law of friction is:

$$\sigma'_{xx} = 2\eta_{eff}\dot{\varepsilon}_{xx} \quad \dot{\varepsilon}_{xx} = \frac{\partial v_x}{\partial x}$$

$$\sigma'_{xz} = 2\eta_{eff}\dot{\varepsilon}_{xz} \quad \dot{\varepsilon}_{xz} = \frac{1}{2}\left(\frac{\partial v_x}{\partial z} + \frac{\partial v_z}{\partial x}\right)$$

$$\sigma'_{zz} = 2\eta_{eff}\dot{\varepsilon}_{zz} \quad \dot{\varepsilon}_{zz} = \frac{\partial v_z}{\partial x}$$

where η_{eff} is the effective viscosity that depends on the pressure, temperature, composition, strain rate and degree of melting.

For rocks containing small melt fractions, the effective viscosity for ductile creep as a function of pressure, temperature, composition and strain rate invariant is defined by:

$$\eta_{ductile} = (\dot{\varepsilon}_{II})^{\frac{1-n}{n}}F(A_D)^{-\frac{1}{n}}exp\left(\frac{E+PV}{RT}\right)$$

where $\dot{\varepsilon}_{II}$ is the second invariant of the strain rate tensor and $A_D A_D$, E, V and n are experimentally determined flow law parameters, which stand for material constant, activation energy, activation volume and stress exponent, respectively, F is a dimensionless coefficient depending on the type of experiments on which the flow law is based. For example, $F=2^{(1-n)/n}/3^{(1+n)/2n}F = \frac{2^{\frac{(1-n)}{n}}}{3^{\frac{(1+n)}{2n}}}$ for triaxial compression and $F=2^{(1-n)/n}$ for simple shear.

The ductile rheology is combined with a brittle/plastic rheology to yield an effective visco-plastic rheology. For this purpose, the Drucker–Prager yield criterion is implemented as follows:

$$\sigma_{yield} = C_o + Psin(\varphi)$$

$$sin(\varphi_{eff}) = sin(\varphi)(1 - \lambda)$$

$$\eta_{plastic} = \frac{\sigma_{yield}}{2\dot{\varepsilon}_{II}}$$

where σ_{yield} is the yield stress $\dot{\varepsilon}_{II}$, P is the dynamic pressure, C_0 is the cohesion, φ is the internal frictional angle, λ is the pore fluid coefficient that controls the brittle strength of fluid-containing porous or fractured media, and φ_{eff} can be illustrated as the effective internal frictional angle that integrates the effects of the initial frictional angle *(φ)* and pore fluid coefficient *(λ)*. In this paper, the plastic rheology is implemented by variable values of $sin(\varphi_{eff})$ for different rock types.

The $\eta_{ductile}$ and $\eta_{plastic}$ visco-plastic rheology are assigned to the model by means of a Christmas tree-like criterion, where the rheological behavior depends on the minimum viscosity (or differential stress) attained between the ductile and brittle/plastic fields, which is further controlled by the cut-off values of (10^{18}–10^{25} Pa s).

$$\eta_{creep} = min(\eta_{ductile}, \eta_{plastic})$$

Model setup

Large-scale numerical models (1800 × 400 km; insets in Fig. 3) were constructed to evaluate geometry of subduction zone in circum-Pacific. The models consist of a non-uniform 201 × 66 rectangular grid with high resolution in the vicinity of the subduction zone but low resolution further away. The numerical models incorporate an oceanic domain on the right and a continental domain on the left. The oceanic domain comprises a sediments layer (1 km thick), oceanic crust (9 km thick), oceanic lithospheric mantle (60 km thick), and underlying asthenospheric mantle. The continental domain consists of the upper crust (20 km thick), lower crust (15 km thick), continental lithospheric mantle (58 km thick) and asthenosphere (Huangfu et al., 2016b). The absolute subduction velocity of the downgoing slab and the absolute trench-ward velocity of the overriding continental lithosphere are assigned to each cases of modeling according to the plate reconstruction of the GPlates. Various ages of oceanic and continental crust are assigned to different modeling according to the reconstruction by GPlates.

The initial thermal structure of lithosphere is simplified to be linearly interpolated with 0 °C at the surface and 1300 °C at the base of the lithospheric mantle (Turcotte and Schubert, 2002). The initial temperature gradient in the asthenospheric mantle is 0.5 °C/km (Huangfu et al., 2016a; Turcotte and Schubert, 2002). The boundary conditions used in the models are free slip at all boundaries (Burg and Gerya, 2005). Mechanical parameters of various rocks are illustrated in Table 1, which can constrain brittle and ductile deformation.

References

Bird, P., 2003. An updated digital model of plate boundaries. Geochem Geophy Geosy 4, 1027.
Bittner, D., Schmeling, H., 1995. Numerical modeling of melting processes and induced diapirism in the lower crust. Geophysical Journal International 123, 59-70.

Burg, J.P., Gerya, T.V., 2005. The role of viscous heating in Barrovian metamorphism of collisional orogens: thermomechanical models and application to the Lepontine Dome in the Central Alps. J Metamorph Geol 23, 75-95.

Clauser, C., Huenges, E., 1995. Thermal Conductivity of Rocks and Minerals, in: Ahrens, T.J. (Ed.), Rock Physics & Phase Relations. American Geophysical Union, pp. 105-126.

Gerya, T.V., Connolly, J.A.D., Yuen, D.A., 2008. Why is terrestrial subduction one-sided? Geology 36, 43-46.

Gerya, T.V., Yuen, D.A., 2003. Characteristics-based marker-in-cell method with conservative finite-differences schemes for modeling geological flows with strongly variable transport properties. Phys Earth Planet In 140, 293–318.

Gerya, T.V., Yuen, D.A., 2007. Robust characteristics method for modelling multiphase visco-elasto-plastic thermo-mechanical problems. Phys Earth Planet In 163, 83-105.

Gurnis, M., Turner, M., Zahirovic, S., DiCaprio, L., Spasojevic, S., Muller, R.D., Boyden, J., Seton, M., Manea, V.C., Bower, D.J., 2012. Plate tectonic reconstructions with continuously closing plates. Comput Geosci 38, 35-42.

Hayes, G.P., Moore, G.L., Portner, D.E., Hearne, M., Flamme, H., Furtney, M., Smoczyk, G.M., 2018. Slab2, a comprehensive subduction zone geometry model. Science 362, 58-61.

Hofmeister, A.M., 1999. Mantle values of thermal conductivity and the geotherm from phonon lifetimes. Science 283, 1699-1706.

Huangfu, P., Li, Z.-H., Gerya, T., Fan, W., Zhang, K.-J., Zhang, H., Shi, Y., 2018. Multi-terrane structure controls the contrasting lithospheric evolution beneath the western and central–eastern Tibetan plateau. Nat Commun 9, 3780.

Huangfu, P.P., Wang, Y.J., Cawood, P.A., Li, Z.H., Fan, W.M., Gerya, T.V., 2016a. Thermo-mechanical controls of flat subduction: Insights from numerical modeling. Gondwana Research 40, 170-183.

Huangfu, P.P., Wang, Y.J., Li, Z.H., Fan, W.M., Zhang, Y., 2016b. Effects of crustal eclogitization on plate subduction/collision dynamics: Implications for India-Asia collision. J Earth Sci-China 27, 727-739.

Li, Z.H., Xu, Z.Q., Gerya, T.V., 2011. Flat versus steep subduction: Contrasting modes for the formation and exhumation of high- to ultrahigh-pressure rocks in continental collision zones. Earth and Planetary Science Letters 301, 65–77.

Matthews, K.J., Maloney, K.T., Zahirovic, S., Williams, S.E., Seton, M., Muller, D., 2016. Global plate boundary evolution and kinematics since the late Paleozoic. Global Planet Change 146, 226-250.

Müller, R.D., Cannon, J., Qin, X.D., Watson, R.J., Gurnis, M., Williams, S., Pfaffelmoser, T., Seton, M., Russell, S.H.J., Zahirovic, S., 2018. GPlates: Building a virtual earth through deep time. Geochem Geophy Geosy 19, 2243-2261.

Müller, R.D., Sdrolias, M., Gaina, C., Roest, W.R., 2008. Age, spreading rates, and spreading asymmetry of the world's ocean crust. Geochem Geophy Geosy 9.

Müller, R.D., Seton, M., Zahirovic, S., Williams, S.E., Matthews, K.J., Wright, N.M., Shephard, G.E., Maloney, K.T., Barnett-Moore, N., Hosseinpour, M., Bower, D.J., Cannon, J., 2016. Ocean basin evolution and global-scale plate reorganization events since Pangea breakup. Annual Review of Earth and Planetary Sciences 44, 107–138.

Ranalli, G., 1995. Rheology of the Earth. Springer Netherlands.

Seton, M., Muller, R.D., Zahirovic, S., Gaina, C., Torsvik, T.H., Shephard, G., Talsma, A., Gurnis, M., Turner, M., Maus, S., Chandler, M., 2012. Global continental and ocean basin reconstructions since 200 Ma. Earth-Science Reviews 113, 212–270.

Turcotte, D.L., Schubert, G., 2002. Geodynamics, 2nd ed. Cambridge University Press, Cambridge.

Zahirovic, S., Flament, N., Muller, R.D., Seton, M., Gurnis, M., 2016. Large fluctuations of shallow seas in low-lying Southeast Asia driven by mantle flow. Geochem Geophy Geosy 17, 3589–3607.